A NEW PRACTICAL WIND ESTIMATION TECHNIQUE FOR UNMANNED HELICOPTERS

Sergey Nazarov
Technion - Israel Institute of Technology
Haifa, Israel

Per-Olof Gutman
Technion - Israel Institute of Technology
Haifa, Israel

ABSTRACT

In this study, the authors propose a new model-based algorithm for atmospheric disturbances estimation using an inertial navigation system and Pitot measurements. The linear model of helicopter dynamics is modified into a quasi-nonlinear model by adding trim data and nonlinear kinematic equations. A nonlinear Kalman filter is designed based on this quasi-nonlinear model, utilizing a scaled Unscented Transformation. The resulting estimate was split using moving averages into sustained horizontal wind and atmospheric fluctuations. The paper presents validation results obtained by flight testing under hover conditions. Wind characteristics were measured with an ultrasonic sensor and the results were compared with the estimates. CIFER software was used to identify the refined gust matrix in the frequency domain. The authors introduced a simple wind dynamics model and incorporated a gust matrix to account for angular velocity components. The results indicate that the estimation of horizontal atmospheric disturbances can be improved with this approach.

NOTATION

Note that regular and bold symbols have different meanings.

*

Symbols

$\boldsymbol{A}, \boldsymbol{B}$ Linear system and control matrices

a_x, a_y, a_z Accelerometer measurements, m/s^2

$\boldsymbol{C}, \boldsymbol{D}$ Measurement and direct term matrices

$\boldsymbol{C}(s)$ Controller transfer function

$\boldsymbol{C}_I^B$ Inertial to body rotational matrix

$\boldsymbol{C}_x$ Cholesky factor

$\boldsymbol{F}$ Continuous nonlinear process function

$\boldsymbol{F}_I$ Total external force, N

$\bar{\boldsymbol{F}}_g, \bar{\boldsymbol{F}}_a$ Specific gravity and aerodynamic forces, m/s^2

$\Delta\boldsymbol{F}_a$ Perturbation of aerodynamic force, N

$\boldsymbol{G}$ Gust matrix

$\boldsymbol{G}_{**}$ One-sided power spectra density

g Acceleration of gravity, m/s^2

$\boldsymbol{H}$ Nonlinear observation function

$\boldsymbol{H}_T$ Total angular momentum, N·m·s

$\boldsymbol{H}_{**}$ Frequency response function

$\boldsymbol{I}$ Inertia tensor, kg·m^2

I_x, I_y, I_z Roll, pitch, yaw moment of inertia, kg·m^2

I_{xz} Product of inertia, kg·m^2

$\boldsymbol{K}$ Kalman gain

K_* Coefficients for the frequency response calculation

k Discrete time

$k_{q_g}^{u_g}, k_{r_g}^{v_g}$ Coupling coefficients in the wind model, s^2/m

$\mathcal{M}$ Mass-inertia tensor, kg, kg·m^2

$\boldsymbol{M}$ Rate matrix

$\boldsymbol{M}_a$ Total aerodynamic moment, N·m

$\boldsymbol{M}_g$ Part of the rate matrix referring to the wind model

M_* Pitch derivatives, 1/s

m Helicopter base mass, kg

m_c Helicopter current mass, kg

$\boldsymbol{n}$ Measurement noise vector

n Size of state vector

P, Q, R Total rates (roll, pitch, yaw), rad/s

P_* Covariance matrix

p, q, r Rate perturbations (roll, pitch, yaw), rad/s

$\boldsymbol{Q}$ Process noise covariance matrix

R Rotor radius, m

$\boldsymbol{R}$ Measurement noise covariance matrix

$\boldsymbol{r}_f$ Reference signal vector

$\boldsymbol{r}$ Aircraft position radius vector, m

$\mathcal{S} = (\mathcal{W}, \boldsymbol{\mathcal{X}})$ Weighted sigma points set

T Data record length

t, t_s Time and sampling interval, s

U, V, W Body velocity components, m/s

$\boldsymbol{U}_d$ Delayed control vector, rad

U_w, V_w, W_w Wind components in the body frame, m/s

u, v, w Body velocity component perturbations, m/s

u_g, v_g, q_g, r_g Linear and angular gusts, m/s, rad/s

$\boldsymbol{V}_B$ Velocity referred to the body axis, m/s

$\boldsymbol{V}_I$ Total inertial velocity, m/s

V_N, V_E, V_D Velocity in the North-East-Down frame, m/s

$V_i, \boldsymbol{V}_a$ Indicated and true airspeed, m/s

$\boldsymbol{V}_{wind}$ Wind referred to the body axis, m/s

$\boldsymbol{v}$ Measurement noise vector

$\boldsymbol{W}$ Navigational wind vector, m/s

$\boldsymbol{W}_0, \boldsymbol{\delta W}$ Sustained wind and turbulence, m/s

$\boldsymbol{W}_{\mathbf{meteo}}$ Meteorological wind vector, kt

W_N, W_E, W_D Wind components in the NED frame, m/s

$\boldsymbol{w}$ Process noise vector

$\boldsymbol{X}, \boldsymbol{U}$ Total state and control vectors

$\boldsymbol{X^a}$ Augmented state vector

Z_w Heave damping stability derivative, 1/s

$\boldsymbol{x}, \boldsymbol{u}$ Perturbed state and control vectors

x, y, z Aircraft position, m

x_a, y_a, z_a IMU position offset, m

$\boldsymbol{y}$ Output vector

$\boldsymbol{Z}$ Measurement vector

$\tilde{\boldsymbol{Z}}$ Innovation vector

β Side-slip angle, deg

β_{1c}, β_{1s} Flap angles for longitudinal and lateral tip path plane, rad

$\Delta\delta_*$ Control signal perturbations, rad

$\delta_{col}, \delta_{ped}$ Collective and pedals controls, rad

$\delta_{lat}, \delta_{lon}$ Cyclic controls, rad

κ_{1c}, κ_{1s} Stabilizer bar flap angles, rad

$\boldsymbol{\tau}$ Equivalent delay vector, s

$\tau_{u_g}, \tau_{v_g}, \tau_{q_g}, \tau_{r_g}$ Time constants in wind model, s

$\boldsymbol{\Phi}$ Discrete nonlinear process function

Φ, Θ, Ψ Absolute attitudes (roll, pitch, yaw), rad

ϕ, θ, ψ Attitude perturbations (roll, pitch, yaw), rad

$\boldsymbol{\omega}$ Angular velocity vector, rad/s

*

Subscripts and Superscripts

0 Relate to the trim conditions

d Relate to the discrete time

e Relate to the extended linear model

*

Acronyms

CG Center of Gravity

DCM Direction Cosine Matrix

ICAO International Civil Organization

IMU Inertial Measurement Unit

INS Inertial Navigation System

GPS Global Positioning System

GS Ground Speed

NED North-East-Down

NTP Network Time Protocol

TAS True Airspeed

UA Unmanned Aircraft

UAS Unmanned Aircraft System

UKF Unscented Kalman Filter

UT Unscented Transformation

INTRODUCTION

The rapid development of civilian unmanned aircraft has raised serious concerns regarding flight safety. According to Circular 328 issued by the International Civil Aviation Organization (ICAO) (Ref. 1), civil Unmanned Aircraft Systems (UAS) must achieve safety levels equivalent to those of manned aircraft. Wind conditions and atmospheric turbulence present significant challenges for helicopter operations. For rotary UAS operating within the lowest boundary layer of the atmosphere, the characteristics, magnitude, and frequency content of atmospheric flow can affect dynamics, control performance, and ultimately safety. Consequently, a precise determination of the wind conditions is essential.

The traditional approach to wind estimation for fixed-wing aircraft utilizes the wind triangle, relying on true airspeed (TAS) obtained from the air data system and ground speed (GS) from the navigation system. In (Ref. 2), circular flight patterns are used to estimate wind speed and direction by minimizing error variance. However, this method assumes that TAS is known, which is often not true for small UAS lacking an air data system. In (Ref. 3), a correction factor based on the angle of attack and sideslip is used, but this approach assumes that these angles are small.

A rare example of wind estimation for a single-rotor helicopter is presented in (Ref. 4), which utilizes a complex nonlinear helicopter model. Particle Swarm Optimization is used to optimize 37 parameters of this model for hover conditions. This optimization is based on the measurement of translational and rotational acceleration. Subsequently, the model extracted the wind parameters through anomalies in the helicopter dynamics estimates. However, this approach appears to have limited practical applicability: in rotorcraft applications, first-principles dynamics modeling involves several analytically uncertain parameters that are difficult to determine (Ref. 5).

Typically, turbulence estimation is considered separately from wind estimation in scientific studies. In the fixed-wing approach to considering atmospheric turbulence for flight dynamics problems, several simplifying assumptions (Ref. 6) are made, and vertical acceleration is used to reconstruct the intensity of the turbulence (Ref. 7). However, standard turbulence models are not always applicable to rotary-wing aircraft due to the different flight regimes and aerodynamic conditions (low airspeed, rotating airfoil) (Ref. 8). For rotorcraft, due to the flapping of the blades, a significant fraction of the turbulence energy is damped and the load factor at the center of gravity is lower than that of a fixed-wing airplane (Ref. 9). However, the loads on the hub increase significantly. These challenges make a turbulence reconstruction from the helicopter response is nontrivial.

The literature on this subject for rotorcraft is sparse. In (Ref. 10), a Kalman filter approach is proposed to identify gusts using a small-scale helicopter. A 28-state linear model of the open-loop helicopter dynamics was extracted from GenHel© for a trim condition (Ref. 11). The model was simplified to a 9-state rigid body dynamics model. Wind gust disturbances are added to the helicopter model by a gust matrix $\boldsymbol{G}$. The terms in the matrix $\boldsymbol{G}$ are substantially different from the equivalent terms in the matrix $\boldsymbol{A}$. However, finding the matrix $\boldsymbol{G}$ can be tricky. Significant modifications were made to the GenHel© model to obtain a linear $\boldsymbol{G}$ matrix. This algorithm yielded positive results on the primary flow axis; however, the gust detection error was significant in the off-axis flow direction.

This research introduces a new in-flight algorithm that utilizes a standard Unmanned Aircraft (UA) sensor kit and the control signals generated by the flight control system as the primary data sources for the wind field reconstruction. Unlike existing methods, this approach does not rely on the assumption of steady flight. As a basic model of helicopter dynamics, a linear identified model is proposed, which is utilized for flight control design and applies to all UAS projects. This linear model is then enhanced into a quasi-nonlinear model by incorporating trim data and nonlinear kinematic equations.

A nonlinear Unscented Kalman filter is developed based on the quasi-nonlinear helicopter model and the scaled Unscented Transformation (UT) to estimate wind components in the North-East-Down (NED) coordinate frame. The resulting estimates are processed using moving averages to distinguish between sustained horizontal wind and atmospheric turbulence. This algorithm was tested and validated by an actual BE-50E helicopter flight test. Validation in hover was performed using measurements from the ultrasonic wind sensor. These measurements were also used for the identification and improvement of the dynamic wind model.

METHODOLOGY

Definition of Wind and Aviation Turbulence

The definitions of wind and turbulence can vary across different scientific fields.Here we clarify the definitions used in this paper. The movement of air within the atmosphere is characterized by inherent turbulence, which encompasses a diverse array of eddy sizes. The larger eddies are distinguished by such significant scales that air movement inside these eddies can be regarded as exhibiting a movement with constant speed from the perspective of flight dynamics. This type of airflow in aviation is termed *steady wind* (Ref. 12), which is assumed to act parallel to the earth's surface. A particular subset of turbulence, which has an impact on an aircraft during flight, is called *aviation turbulence* (Ref. 13). Therefore, the aircraft's reaction determines the spectrum of atmospheric fluctuations of interest, and aviation turbulence refers to the conditional atmospheric fluctuations expressed in meters per second that cause the aircraft to react accordingly.

Let us denote $\boldsymbol{r}(x, y, z, t)$ as the radius vector defining the position of the rotorcraft relative to a specific point on the earth's surface. The wind affecting the rotorcraft flight dynamics can be defined as

$$\boldsymbol{W}(\boldsymbol{r}, t) = \boldsymbol{W}_0(\boldsymbol{r}, t) + \boldsymbol{\delta W}(\boldsymbol{r}, t) \tag{1}$$

where $\boldsymbol{W}_0(\boldsymbol{r}, t)$ characterizes a very slowly varying component, which refers to the *sustained wind* (Ref. 14), and

$\boldsymbol{\delta W}(\boldsymbol{r}, t)$ is a random component with constant statistical characteristics.

For convenience, we use the navigational wind vector in the North-East-Down frame in the process model,

$$\boldsymbol{W} = \begin{bmatrix} W_N & W_E & W_D \end{bmatrix}^T \tag{2}$$

which can be converted into body frame $\boldsymbol{V}_{\text{wind}}$ using a transformation matrix $\boldsymbol{C}_I^B$. The sustained wind component is defined as the movement of air parallel to the earth's surface $\boldsymbol{W}_0 = \begin{bmatrix} W_{N_0} & W_{E_0} & 0 \end{bmatrix}$. It can be obtained from $\boldsymbol{W}(t)$ by averaging over a specific time (Ref. 14).

The final goal of our wind estimation is to obtain the direction of the meteorological wind $\angle \boldsymbol{W}_{\text{meteo}}$ and the speed $|\boldsymbol{W}_{\text{meteo}}|$, where the meteorological wind is defined as

$$\boldsymbol{W}_{\text{meteo}} = -\boldsymbol{W}_0 \tag{3}$$

Aviation turbulence $\boldsymbol{\delta W}(t)$ can be represented by statistical characteristics for a selected period, both in the coordinate system with the X-axis aligned with the wind direction or in the body axes of the helicopter. In the first case, $\boldsymbol{\delta W}$ needs to be rotated by a wind angle, and in the second case, through the DCM transformation. After that, the moving variance can be applied. Note that the vertical components in $\boldsymbol{W}$ and $\boldsymbol{\delta W}$ are identical.

Equations of Motion

The rotorcraft's position relative to the inertial coordinate system is described by the differential equation

$$\frac{\mathrm{d}\boldsymbol{r}}{\mathrm{d}t} = \boldsymbol{V}_I(t) = \boldsymbol{V}_a(t) + \boldsymbol{W}(\boldsymbol{r}, t) \tag{4}$$

where $\boldsymbol{V}_I$ is the inertial velocity, $\boldsymbol{V}_a$ is the true airspeed and $\boldsymbol{W}$ is the wind vector. All velocities here are defined relative to the rotorcraft's center of gravity (CG). Newton's second law describes the rotorcraft's CG translational motion as

$$\frac{\mathrm{d}(m\boldsymbol{V}_I)}{\mathrm{d}t} = \boldsymbol{F}_I \tag{5}$$

where $\boldsymbol{F}_I$ is the total external force vector in the inertial frame.

The velocity vector referred to the body frame is related to the inertial velocity vector through the direction cosine matrix (DCM) $\boldsymbol{C}_I^B$, which is determined by the Euler angles: roll Φ, pitch Θ, and yaw Ψ.

$$\boldsymbol{V}_B = \boldsymbol{C}_I^B \boldsymbol{V}_I \tag{6}$$

$$\boldsymbol{C}_I^B = \begin{bmatrix} c\Psi c\Theta, & s\Psi c\Theta, & -s\Theta \\ c\Psi s\Theta s\Phi - s\Psi c\Phi, & s\Psi s\Theta s\Phi + c\Psi c\Phi, & c\Theta s\Phi \\ c\Psi s\Theta c\Phi + s\Psi s\Phi, & s\Psi s\Theta c\Phi - c\Psi s\Phi, & c\Theta c\Phi \end{bmatrix} \tag{7}$$

where c and s denote the cosine and sine functions. For a body-fixed coordinate system, the equation Eq. 5 can be rewritten as

$$\frac{\partial \boldsymbol{V}_B}{\partial t} + \boldsymbol{\omega} \times \boldsymbol{V}_B = \bar{\boldsymbol{F}}_g + \bar{\boldsymbol{F}}_a \tag{8}$$

where $\boldsymbol{V}_B = U\boldsymbol{i} + V\boldsymbol{j} + W\boldsymbol{k}$ is the velocity vector expressed in components in the body axis, $\boldsymbol{\omega} = P\boldsymbol{i} + Q\boldsymbol{j} + R\boldsymbol{k}$ is the angular velocity vector of the body-fixed axis system, $\bar{\boldsymbol{F}}_g$ is specific gravity which is a function of the angular orientation of the rotorcraft relative to the earth's surface,

$$\bar{\boldsymbol{F}}_g = \begin{bmatrix} -g\sin\Theta \\ g\sin\Phi\cos\Theta \\ g\cos\Phi\cos\Theta \end{bmatrix} \tag{9}$$

and $\bar{\boldsymbol{F}}_a$ is the aerodynamic force in the body frame.

The moment equation expressed in a body-fixed frame is

$$\frac{\partial \boldsymbol{H}_T}{\partial t} + (\boldsymbol{\omega} \times \boldsymbol{H}_T) = \boldsymbol{M}_a \tag{10}$$

where $\boldsymbol{H}_T = \boldsymbol{I}\,\boldsymbol{\omega}$ is a total angular momentum, $\boldsymbol{I}$ is an inertia tensor

$$\boldsymbol{I} = \begin{bmatrix} I_x & 0 & -I_{xz} \\ 0 & I_y & 0 \\ -I_{zx} & 0 & I_z \end{bmatrix} \tag{11}$$

and $\boldsymbol{M}_a$ is a vector of total aerodynamic moment. The Euler rates in terms of the roll, pitch, and yaw rates are expressed as

$$\begin{bmatrix} \dot{\Phi} \\ \dot{\Theta} \\ \dot{\Psi} \end{bmatrix} = \frac{1}{\cos\Theta} \begin{bmatrix} \cos\Theta, & \sin\Phi\sin\Theta, & \cos\Phi\sin\Theta \\ 0, & \cos\Phi\cos\Theta, & -\sin\Phi\cos\Theta \\ 0, & \sin\Phi, & \cos\Phi \end{bmatrix} \begin{bmatrix} P \\ Q \\ R \end{bmatrix} \tag{12}$$

The specific aerodynamic force $\bar{\boldsymbol{F}}_a(\boldsymbol{V}_a)$ and the vector of the total aerodynamic moment $\boldsymbol{M}_a(\boldsymbol{V}_a)$ are functions of the true airspeed due to the basic aerodynamics. Suppose that we can model aerodynamic forces and moments as functions of airspeed. In that case, we can use Eqs. 4 - 12 as a Kalman filter nonlinear process model to estimate the wind $\boldsymbol{W}(t)$. This model is part of the helicopter flight dynamics model. The main goal of unmanned helicopter dynamics modeling is flight control design, for which it is standard practice to use linear models. The numerical values of the stability and control derivatives were provided by Steadicopter Ltd. and are not part of this paper.

Aerodynamic Force and Moment Calculation

The linearized equations of the rotorcraft motion realized in the state-space form are

$$\dot{\boldsymbol{x}}(t) = \boldsymbol{A}\boldsymbol{x}(t) + \boldsymbol{B}\boldsymbol{u}(t - \boldsymbol{\tau}) \tag{13}$$

where a time-delay vector $\boldsymbol{\tau}$ expresses the unmodeled high-order dynamics and the equivalent delay in the electrical part of the control system.

The size of the state vector depends on the specific dynamics of a particular helicopter. Typically, small-scale helicopters have low-damping coupled fuselage-rotor flapping dynamics, and a coupled rotor-body model is required. The state and control vectors used in Eq. 13 are

$$\begin{aligned} \boldsymbol{x} &= \begin{bmatrix} u & v & w & p & q & r & \phi & \theta & \psi & \beta_{1c} & \beta_{1s} & \kappa_{1c} & \kappa_{1s} \end{bmatrix}^T \\ \boldsymbol{u} &= \begin{bmatrix} \Delta\delta_{ped} & \Delta\delta_{lat} & \Delta\delta_{lon} & \Delta\delta_{col} \end{bmatrix}^T \end{aligned} \tag{14}$$

where u, v and w are perturbations of axial, lateral, and normal velocity perturbations; p, q and r are the roll, pitch, and yaw rate perturbations; ϕ, θ and ψ are perturbations of Euler angles; β_{1c} and β_{1s} are the rotor flap angles for the longitudinal and lateral tip path plane and κ_{1c} and κ_{1s} stabilizer bar flap angles. Throughout the article, lowercase letters denote state perturbations, while uppercase letters represent total signals (for example, θ and Θ). We use Δ to denote perturbations in the control signal. For convenience, we use the indices commonly used for manned helicopters for controls (pedals δ_{ped}, collective δ_{col}, longitudinal δ_{lon}, and lateral cyclic δ_{lat}).

The procedure for calculating aerodynamic forces and moments from the identified linear model is similar to the algorithm used in the model stitching simulation (Ref. 15). From the identified model, we used only the stability and control derivatives associated with the aerodynamic forces and moments to calculate the linear and angular accelerations. These accelerations, when multiplied by the mass/inertia matrix, yield perturbations of the aerodynamic forces and the total aerodynamic moments.

$$\begin{bmatrix} \Delta\boldsymbol{F}_a \\ \boldsymbol{M}_a \end{bmatrix} = \mathcal{M}\Big[\boldsymbol{A}_{66}\boldsymbol{x}_6 + \boldsymbol{A}_{6H}\boldsymbol{x}_H + \boldsymbol{B}_6\boldsymbol{u}\,(t-\boldsymbol{\tau})\Big] \tag{15}$$

where $\mathcal{M}$ is a mass-inertia tensor, $\boldsymbol{A}_{66}$ is the part of $\boldsymbol{A}$ matrix associated with the state

$$\boldsymbol{x}_6 = \begin{bmatrix} u & v & w & p & q & r \end{bmatrix} \tag{16}$$

from which all derivatives relating to inertial forces have been removed, $\boldsymbol{B}_6$ is the corresponding part of $\boldsymbol{B}$, and $\boldsymbol{A}_{6H}$ is the corresponding part of $\boldsymbol{A}$ associated with $\boldsymbol{x}_6$ and the high order states.

$$\boldsymbol{x}_H = \begin{bmatrix} \beta_{1c} & \beta_{1s} & \kappa_{1c} & \kappa_{1s} \end{bmatrix} \tag{17}$$

To obtain the total specific aerodynamic force vector, we should add its trim value, which numerically equals the gravity force with opposite sign in the trim flight (see Eq. 9).

$$\bar{\boldsymbol{F}}_a = \frac{1}{m_c}\Delta\boldsymbol{F}_a - \bar{\boldsymbol{F}}_{g_0} \tag{18}$$

where m_c is the helicopter current mass. The process of calculation $\bar{\boldsymbol{F}}_a$ and $\boldsymbol{M}_a$ from the linear model is more detailed in our previous article (Ref. 16).

The Quasi-Nonlinear Helicopter Dynamics Model

The basic idea of the quasi-nonlinear model is to calculate the vectors of the specific aerodynamic force $\bar{\boldsymbol{F}}_a$ and the total aerodynamic moment $\boldsymbol{M}_a$ from a linear model as described in the previous Section and then use the equations of motion in their natural nonlinear form. The quasi-nonlinear model consists of nonlinear equations of motion and a linear model for high-order states,

$$\dot{\boldsymbol{x}}_H(t) = \boldsymbol{A}_{H6}\boldsymbol{x}_6(t) + \boldsymbol{A}_{HH}\boldsymbol{x}_H(t) + \boldsymbol{B}_H\boldsymbol{u}\,(t-\boldsymbol{\tau}) \tag{19}$$

where the $\boldsymbol{A}_{H6}$, $\boldsymbol{A}_{HH}$ and $\boldsymbol{B}_H$ parts of the matrices $\boldsymbol{A}$ and $\boldsymbol{B}$ in Eq. 13 refer to the flaps of the blade and stabilizer bar. We denote the quasi-nonlinear model as follows.

$$\dot{\boldsymbol{X}}(t) = \boldsymbol{F}\big\{\boldsymbol{X}(t), \boldsymbol{U}(t-\boldsymbol{\tau})\big\} \tag{20}$$

where $\boldsymbol{X}$ is the vector of the total states except for the flapping angles and $\boldsymbol{U}$ is the vector of the total controls.

$$\begin{aligned} \boldsymbol{X} &= \begin{bmatrix} U & V & W & P & Q & R & \Phi & \Theta & \Psi & \beta_{1c} & \beta_{1s} & \kappa_{1c} & \kappa_{1s} \end{bmatrix}^T, \\ \boldsymbol{U} &= \begin{bmatrix} \delta_{ped} & \delta_{lat} & \delta_{lon} & \delta_{col} \end{bmatrix}^T \end{aligned} \tag{21}$$

However, the linear equation Eq. 19 and the computation of aerodynamic forces and moments Eq. 15 both utilize perturbations of the state and control vectors.

$$\begin{aligned} \boldsymbol{x} &= \boldsymbol{X} - \boldsymbol{X}_0 \\ \boldsymbol{u} &= \boldsymbol{U} - \boldsymbol{U}_0 \end{aligned} \tag{22}$$

where $\boldsymbol{X}_0$ and $\boldsymbol{U}_0$ the state and control vectors in trim conditions. These are the vectors for which the model Eq. 13 was linearized.

Atmospheric Disturbances - Helicopter Interface

The dynamic response of the aircraft to wind depends on the vehicle's speed and can be quite complex. The expression Eq. 23 defines the total time derivative of the wind velocity at the point moving with velocity $\boldsymbol{V}_I$.

$$\frac{d\boldsymbol{W}}{dt} = \frac{\partial\boldsymbol{W}}{\partial t} + \boldsymbol{V}_I\frac{\partial\boldsymbol{W}}{\partial\boldsymbol{r}} \tag{23}$$

This work assumes that the wind velocity is uniformly distributed over the rotor disk. This assumption is valid for the appropriate ratio of the turbulence length scale and the radius of the rotor (Ref. 17). In this case, we can define the turbulence input as it is used in fixed-wing problems, which utilize the relative velocity vector to calculate the aerodynamics of the aircraft.

$$[\,U\ V\ W\,]^T_{rel} = \boldsymbol{V}_B - \boldsymbol{V}_{\text{wind}} \tag{24}$$

where $\boldsymbol{V}_{\text{wind}} = [\ U_w \quad V_w \quad W_w\ ]^T$ is the wind referred to the body frame.

Unscented Kalman Filter

The Unscented Kalman Filter (UKF) utilizes the Unscented Transform for the nonlinear propagation of the state variables and measurements (Ref. 18). Let us define the discretized process as a nonlinear function of the state $\boldsymbol{X}$ and control $\boldsymbol{U}$ vectors and the nonlinear observation model.

$$\begin{cases} \boldsymbol{X}(k{+}1) = \boldsymbol{\Phi}\big\{\boldsymbol{X}(k), \boldsymbol{U}(k)\big\} + \boldsymbol{w}_d(k) \\ \boldsymbol{Z}(k{+}1) = \boldsymbol{H}\big\{\boldsymbol{X}(k{+}1), \boldsymbol{U}(k)\big\} + \boldsymbol{v}_d(k{+}1) \end{cases} \tag{25}$$

We assume that the distribution of $\boldsymbol{X}(k)$ is Gaussian at any time k, and the discrete noises $\boldsymbol{w}_d(k)$ and $\boldsymbol{v}_d(k)$ are uncorrelated Gaussian white sequences.

$$\begin{gathered} \mathbb{E}\left[\boldsymbol{w}_d(k)\right] = \boldsymbol{0}, \quad \mathbb{E}\left[\boldsymbol{v}_d(k)\right] = \boldsymbol{0} \\ \mathbb{E}\left[\boldsymbol{w}_d(i)\boldsymbol{v}_d(j)^T\right] = \boldsymbol{0} \\ \mathbb{E}\left[\boldsymbol{w}_d(i)\boldsymbol{w}_d(j)^T\right] = \boldsymbol{Q}(i)\delta_{ij} \\ \mathbb{E}\left[\boldsymbol{v}_d(i)\boldsymbol{v}_d(j)^T\right] = \boldsymbol{R}(i)\delta_{ij} \end{gathered} \tag{26}$$

The Kalman filter propagation of two moments of the distribution of $\boldsymbol{X}(k)$ incorporates linearly the measurements at the next time step.

$$\begin{cases} \hat{\boldsymbol{X}}(k{+}1|k{+}1) \;=\; \hat{\boldsymbol{X}}(k{+}1|k) \;+\; \boldsymbol{K}(k{+}1)\tilde{\boldsymbol{Z}}(k{+}1|k) \\ \boldsymbol{P}_x(k{+}1,k{+}1) = \boldsymbol{P}_x(k{+}1|k) \;- \\ \qquad\qquad -\boldsymbol{K}(k{+}1)\boldsymbol{P}_{\tilde{z}}(k{+}1|k)\boldsymbol{K}^T(k{+}1) \end{cases} \tag{27}$$

where $\tilde{\boldsymbol{Z}}(k{+}1|k)$ is the innovation with covariance $\boldsymbol{P}_{\tilde{z}}(k+1|k)$

$$\tilde{\boldsymbol{Z}}(k{+}1|k) = \boldsymbol{Z}(k{+}1) - \hat{\boldsymbol{Z}}(k{+}1|k) \tag{28}$$

and $\boldsymbol{K}$ is the Kalman gain;

$$\boldsymbol{K}(k{+}1) = \boldsymbol{P}_{xz}(k{+}1|k)\boldsymbol{P}_{\tilde{z}}^{-1}(k{+}1|k) \tag{29}$$

where $\boldsymbol{P}_{xz}$ is the predicted cross-correlation matrix between $\hat{\boldsymbol{X}}(k+1|k)$ and $\hat{\boldsymbol{Z}}(k+1|k)$.

The $\boldsymbol{\Phi}$ and $\boldsymbol{H}$ in Eq. 25 are nonlinear function. Therefore, the predictions of state $\hat{\boldsymbol{X}}(k+1|k)$, measurement $\hat{\boldsymbol{Z}}(k+1|k)$ and covariances $\boldsymbol{P}_x(k+1|k)$, $\boldsymbol{P}_{\tilde{z}}(k+1|k)$, $\boldsymbol{P}_{xz}(k+1|k)$ can be calculated using the UT. To do this, we should first define a set of sigma points $\mathcal{S} = (\mathcal{W}, \boldsymbol{\mathcal{X}})$ that characterize the distribution of the state vector $\boldsymbol{X}(k)$ (Ref. 19).

$$\begin{aligned} \boldsymbol{\mathcal{X}}_0 &= \hat{\boldsymbol{X}}(k|k) \\ \boldsymbol{\mathcal{X}}_i &= \hat{\boldsymbol{X}}(k|k) + \sqrt{n+1}\,\boldsymbol{C}_{\boldsymbol{x}}(i) \quad 1 \le i \le n \\ \boldsymbol{\mathcal{X}}_i &= \hat{\boldsymbol{X}}(k+1|k) - \sqrt{n+1}\,\boldsymbol{C}_{\boldsymbol{x}}(i) \quad n+1 \le i \le 2n \end{aligned} \tag{30}$$

where n is the dimension of the state vector and $\boldsymbol{C}_{\boldsymbol{x}}$ is the Cholesky factor.

$$\boldsymbol{P}_x(k|k) = \boldsymbol{C}_x\boldsymbol{C}_x^T \tag{31}$$

The weights are defined as

$$\begin{aligned} \mathcal{W}_0 &= 1/(n+1) \\ \mathcal{W}_i &= 0.5/(n+1) \end{aligned} \tag{32}$$

such that $\sum_0^{2n}\mathcal{W}_i = 1$.

Once the set of weighted sigma points $\mathcal{S} = (\mathcal{W}, \boldsymbol{\mathcal{X}})$ has been derived, the prediction is straightforward (Ref. 20). We transform each sigma point through the process and the observation model,

$$\begin{aligned} \boldsymbol{\mathcal{X}}_i(k+1|k) &= \boldsymbol{\Phi}\{\boldsymbol{\mathcal{X}}_i(k|k), \boldsymbol{U}(k)\} \\ \mathcal{Z}_i(k+1|k) &= \boldsymbol{H}\{\boldsymbol{\mathcal{X}}_i(k+1|k), \boldsymbol{U}(k)\} \end{aligned} \tag{33}$$

and calculate predictions of mean and observation.

$$\begin{aligned} \hat{\boldsymbol{X}}(k+1|k) &= \sum_{i=0}^{2n}\mathcal{W}_i\boldsymbol{\mathcal{X}}_i(k+1|k) \\ \hat{\boldsymbol{Z}}(k+1|k) &= \sum_{i=0}^{2n}\mathcal{W}_i\mathcal{Z}_i(k+1|k) \end{aligned} \tag{34}$$

The prediction of covariance is

$$\boldsymbol{P}_x(k+1|k) = \sum_{i=0}^{2n}\mathcal{W}_i\tilde{\boldsymbol{\mathcal{X}}}_i(k+1|k)\left[\tilde{\boldsymbol{\mathcal{X}}}_i(k{+}1|k)\right]^T + \boldsymbol{Q}(k) \tag{35}$$

Figure 1. BE-50E helicopter

Table 1. BE-50 Main Characteristics

Parameter	English	Metric
Maximum takeoff weight	110 lb	50 kg
Maximum payload weight	33 lb	15 kg
Main rotor diameter	9.2 ft	2.8 m
Total length	10 ft	3.1 m
Max air speed	77 kt	40 m/s
Cruising speed	45 kt	23 m/s
Wind (takeoff and landing)	25 kt	13 m/s

where $\tilde{\boldsymbol{\mathcal{X}}}_i(k+1|k) = \boldsymbol{\mathcal{X}}_i(k+1|k) - \hat{\boldsymbol{X}}(k+1|k)$. Innovation covariance and cross-correlation matrix are calculated in a similar way

$$\boldsymbol{P}_z(k+1|k) = \sum_{i=0}^{2n}\mathcal{W}_i\tilde{\mathcal{Z}}_i(k+1|k)\left(\tilde{\mathcal{Z}}_i(k+1|k)\right)^T \tag{36}$$

$$\boldsymbol{P}_{xz}(k+1|k) = \sum_{i=0}^{2n}\mathcal{W}_i\boldsymbol{\mathcal{X}}_i\left(\tilde{\mathcal{Z}}_i(k+1|k)\right)^T \tag{37}$$

where $\tilde{\mathcal{Z}}_i(k+1|k) = \mathcal{Z}_i(k+1|k) - \hat{\boldsymbol{Z}}(k+1|k)$.

Test Helicopter

The rotary UA used for the research is the BE-50E, manufactured by Steadicopter Ltd., Israel. All supported operations, including flight testing, implementation of suggested control actions, and path patterns, are provided by Steadicopter engineers and pilots. The BE-50E uses a two-bladed teetering main rotor with a Bell-Hiller stabilizer bar (see Figure 1). The main characteristics of the helicopter are given in Table 1.

WIND ESTIMATION ALGORITHM

Nonlinear Process Model

We define an augmented state as the state of a quasi-nonlinear model (see Eq. 21) with the wind vector in the local axes.

$$\boldsymbol{X^a} = \begin{bmatrix} \boldsymbol{X}^T & W_N & W_E & W_D \end{bmatrix}^T \tag{38}$$

The nonlinear process function is

$$\dot{\boldsymbol{X}}^{\boldsymbol{a}}(t) = \boldsymbol{F}\left\{\boldsymbol{X^a}(t), \boldsymbol{U}(t-\boldsymbol{\tau})\right\} + \boldsymbol{w}(t) \tag{39}$$

where $\boldsymbol{w}$ is an additive process noise and $\dot{\boldsymbol{X}}^{\boldsymbol{a}}$ is assumed to have the following form.

$$\dot{\boldsymbol{X}}^{\boldsymbol{a}} = \begin{bmatrix} \dot{\boldsymbol{X}}^T & 0 & 0 & 0 \end{bmatrix}^T \tag{40}$$

The nonlinear transformation $\boldsymbol{F}$ consists of calculating the following equations.

1. DCM (Eq. 7)
2. Wind in body frame $\boldsymbol{V}_{\text{wind}} = \boldsymbol{S}_I^B \boldsymbol{W}$
3. Relative velocity (Eq. 24)
4. Perturbation of state and control vectors (Eq. 22)
5. Specific forces (Eqs. 9, 18) and total aerodynamic moment (Eq. 15)
6. Nonlinear equations of motion (Eqs. 8, 10 and 12)
7. Linear equations of flapping (Eq. 19)

Nonlinear Observation

The measurement vector consists of the INS/GPS and Pitot data.

$$\boldsymbol{Z} = \begin{bmatrix} P \ Q \ R \ a_x \ a_y \ a_z \ \Theta \ \Phi \ \Psi \ V_i \ V_N \ V_E \ V_D \end{bmatrix}^T \tag{41}$$

where $[a_x \ \ a_y \ \ a_z]$ are the measured accelerations, V_i is the indicated air speed, and $\boldsymbol{V}_I = [V_N \ \ V_E \ \ V_D]^T$ is the inertial velocity in the NED frame. The nonlinear observation function is

$$\boldsymbol{Z}(t) = \boldsymbol{H}\left\{\boldsymbol{X}^{\boldsymbol{a}}(t), \boldsymbol{U}(t-\boldsymbol{\tau})\right\} + \boldsymbol{v}(t) \tag{42}$$

where $\boldsymbol{v}$ is an additive measurement noise. Some components of the state vector are measured directly. The velocities in the body coordinate system are related to the inertial velocity in the NED frame through Eq. 6. The accelerometer measurements relative to the helicopter center of gravity are (Ref. 21).

$$\begin{aligned} a_x &= \dot{U} + WQ - VR - \bar{X}_g + z_a\dot{Q} - y_a\dot{R} \\ a_y &= \dot{V} + UR - WP - \bar{Y}_g - z_a\dot{P} + x_a\dot{R} \\ a_z &= \dot{W} + VP - UQ - \bar{Z}_g + y_a\dot{P} - x_a\dot{Q} \end{aligned} \tag{43}$$

where x_a, y_a and z_a are the offsets of the IMU location relative to CG. The indicated speed corresponds to the relative velocity in the X-body direction.

$$V_i = U - U_w \tag{44}$$

Estimation Problem Definition

First, let us discretize the process and the observation for a specific time step $\Delta t = t_s$.

$$\begin{cases} \boldsymbol{X}^{\boldsymbol{a}}(k{+}1) = \boldsymbol{\Phi}\left\{\boldsymbol{X}^{\boldsymbol{a}}(k), \boldsymbol{U}_d(k)\right\} + \boldsymbol{w}_d(k) \\ \boldsymbol{Z}(k{+}1) = \boldsymbol{H}\left\{\boldsymbol{X}^{\boldsymbol{a}}(k{+}1), \boldsymbol{U}_d(k)\right\} + \boldsymbol{v}_d(k{+}1) \end{cases} \tag{45}$$

where $\boldsymbol{U}_d(k)$ is the control vector $\boldsymbol{U}(k)$ delayed by the vector $\boldsymbol{\tau}$.

Summary of UKF algorithm

The implementation of the UKF for wind estimation consists of the following steps.

1. Filter initialization. We initialize with

$$\boldsymbol{X}_0 = \begin{bmatrix} U_0 \ 0 \ W_0 \ 0 \ 0 \ 0 \ \Phi_0 \ \Theta_0 \ \Psi_0 \ 0 \ 0 \end{bmatrix}^T$$
$$\bar{\boldsymbol{X}}(0) = \mathbb{E}\left[\boldsymbol{X}_0\right]$$
$$\boldsymbol{P}_0 = \text{Cov}\left\{\boldsymbol{X}_0\right\}$$
$$\bar{\boldsymbol{X}}^{\boldsymbol{a}}(0) = \begin{bmatrix} \boldsymbol{X}_0^T & 0 & 0 & 0 \end{bmatrix}^T$$
$$\boldsymbol{P}_x(0) = \begin{bmatrix} \boldsymbol{P}_0 & 0 \\ 0 & \boldsymbol{P}_w(0) \end{bmatrix}$$

   where $\boldsymbol{P}_w$ is a covariance of the wind components. During initialization, the control vector $\boldsymbol{U}_d(k)$ is delayed by the vector $\boldsymbol{\tau}$.

2. Calculation of the sigma point set.
3. Prediction.
4. Filtering.

VALIDATION BY FLIGHT TESTING

In our paper (Ref. 16), we presented the results of the validation of the proposed wind estimation method using simulations. We also described the results of the actual 30 Kt helical flight. However, the model-stitching simulation was based on the same model used in the nonlinear process of the Unscented Kalman Filter, and we did not have data to compare with the flight test results. To address this, we conducted a flight test using an ultrasonic sensor to measure the wind. Since the sensor was stationary, the helicopter was operating in hover mode during the test.

Flight Test Installation

When planning the test, we were constrained by the maximum height to which the sensor could be raised. To avoid a ground effect, the sensor was raised to a height of 4.5 meters. It is pretty higher than the required $2R = 2.8$ meters (Ref. 22, p. 259). The helicopter's rotor hub was at the height of the ultrasonic sensor and about five meters away along the wind direction line. Thus, all eddies first reached the sensor and then, with a delay equal to the distance divided by the average wind speed, the helicopter rotor (see Figure 2). The helicopter was turned in the wind with an approximate slip angle $\beta = 40$ degrees.

The helicopter used in the flight test was 20% heavier than the helicopter for which the model Eq. 13 was identified. The difference in weight was accounted for in Eq. 18.

We used a WindMaster Pro sensor from Gill Instruments, which has a measurement resolution of 0.01 m/s. The sensor was configured to operate in the 'UVW' mode with a data rate of 32 Hz. The sensor data was recorded on a laptop. Synchronization with the onboard logger data was performed using GPS time and Network Time Protocol (NTP) on the laptop.

Figure 2. Flight test with a wind sensor

Flight Test Results

We ran two six-minute flight tests, one after the other. The first test was conducted with open-loop manual control and the pilot was instructed to interfere with the controls as little as possible. The second test was conducted in automatic mode, with the control loops tightly closed.

The open-loop estimation results are presented in Figure 3, and the closed-loop results are shown in Figure 4. The results appear to be acceptable. It should be noted that the helicopter is positioned 5 meters away from the sensor and the average wind speed is not constant. Consequently, the eddies reach the helicopter at varying times, and some of them also change shape.

The comparison in the frequency domain is more informative (see Figure 5). The vertical wind component is well estimated up to a frequency of 10 rad/s, while the horizontal component is estimated up to 2 rad/s. Since we estimate the wind from fluctuations in the aerodynamic forces and moments in the body axes, let us examine the frequency response in the helicopter axes (see Figure 6). We observe that the wind component in the X-axis is reasonably well estimated up to 20 rad/s, whereas the lateral wind component is only estimated up to 2 rad/s. Then, this error is transferred to the horizontal NED component through the DCM transformation.

Atmospheric fluctuations are incorporated into our model through the relative state vector (Eq. 24). It is equivalent to using the gust matrix $\boldsymbol{G}$ in the linear model Eq. 13 that contains the first three columns of matrix $\boldsymbol{A}$. This matrix includes the speed derivatives and refers to the slow modes of the flight dynamics. For example, the stability derivative Z_w refers to the first-order heave damping characteristics that are dominant at low frequencies (for full-scale rotorcraft below 1 rad/s, (Ref. 21)). For the small-scale helicopter, as we see in Figure 6c, this dynamic is neat up to 10 rad/s.

We used the linear model (Eq. 13) to compute the fluctuations of the aerodynamic forces and moments. However, this model does not account for specific helicopter dynamics, such as dynamic inflow, engine model, main rotor torque, and tail rotor dynamics, as well as the corresponding effects of wind gusts on these modes. The used gust matrix also does not account for the impact of wind gusts on high-order dynamics, such as blade flapping. The reasons mentioned above can explain the mismatch in the estimates of the side wind component at mid- and high-frequency (Fig. 6b). The longitudinal wind component is better estimated because we use a direct Pitot measurement.

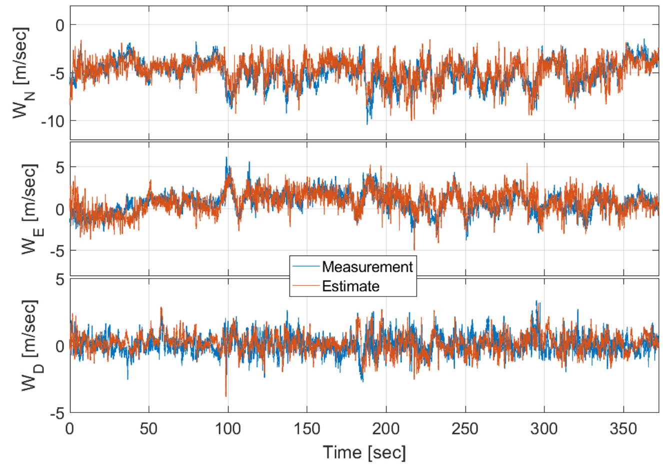

Figure 3. Open-loop test. Time domain

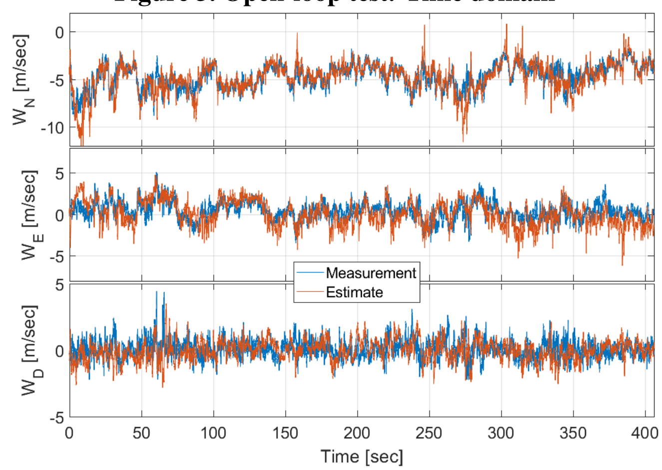

Figure 4. Closed-loop test. Time domain

GUST-HELICOPTER MODEL IDENTIFICATION

Dynamic Turbulence Model

Earlier, we assumed that the wind had no dynamics. Now, we introduce simple wind dynamics and, for this purpose, define new states. In this work, we introduce the dynamics for the horizontal wind component only $\begin{bmatrix} u_g & v_g \end{bmatrix}^T$, which are equal in steady state to the wind vector in the helicopter body axes $\boldsymbol{V}_{\text{wind}}$, taken with a negative sign.

$$\begin{bmatrix} \tau_{u_g} & 0 \\ 0 & \tau_{v_g} \end{bmatrix} \begin{bmatrix} \dot{u}_g \\ \dot{v}_g \end{bmatrix} = \begin{bmatrix} -1 & 0 \\ 0 & -1 \end{bmatrix} \begin{bmatrix} u_g \\ v_g \end{bmatrix} - \begin{bmatrix} U_w \\ V_w \end{bmatrix} \tag{46}$$

In addition, we also introduce the gust angular velocity components.

$$\begin{bmatrix} \tau_{q_g} & 0 \\ 0 & \tau_{r_g} \end{bmatrix} \begin{bmatrix} \dot{q}_g \\ \dot{r}_g \end{bmatrix} = \begin{bmatrix} -1 & 0 \\ 0 & -1 \end{bmatrix} \begin{bmatrix} q_g \\ r_g \end{bmatrix} \tag{47}$$

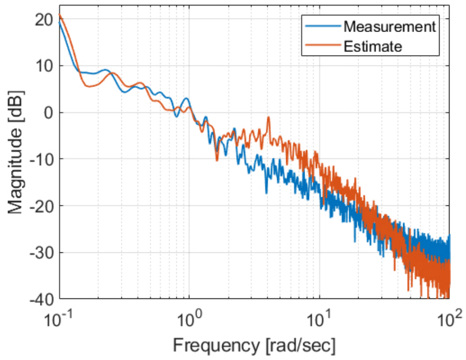

(a) North wind component

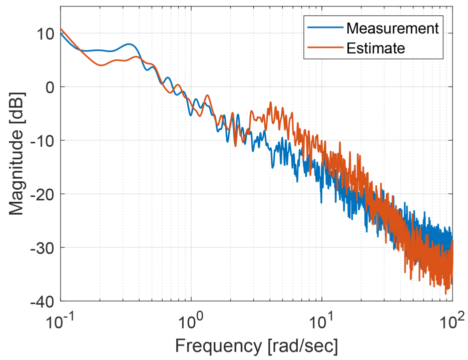

(b) East wind component

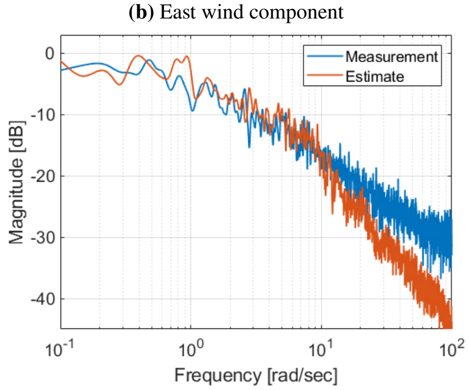

(c) Vertical wind component

Figure 5. Open-loop test. NED

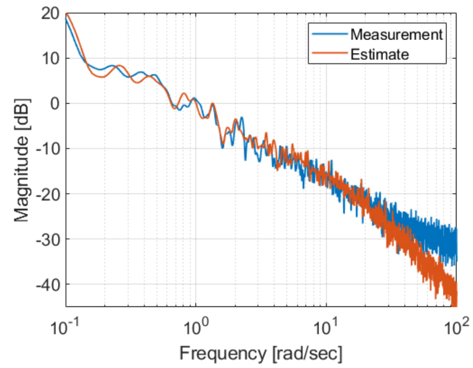

(a) X component

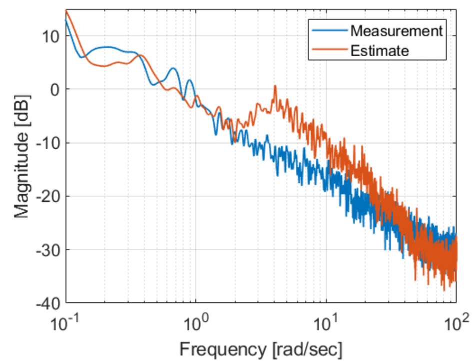

(b) Y component

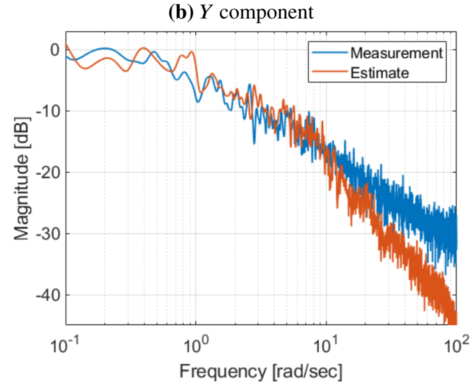

(c) Z component

Figure 6. Open-loop test. Body frame

It should be noted that the angular gusts q_g and r_g differ in meaning from those in the Dryden model, where they represent variations of the linear velocity components along the different aircraft axes. In our model, these components reflect the effect of linear wind gusts on pitch and yaw moments.

The wind in the body axes is used in Eq. 23 to calculate the relative velocity and further calculate the aerodynamic forces and moments. Experiments show that this method for estimating atmospheric disturbances is accurate to 2 rad/s in the lateral direction. Since the vector $\boldsymbol{V}_{\text{wind}}$ has already been used, we will introduce only the derivatives of the new states to calculate the aerodynamic forces and moments.

Let us introduce the gust matrix $\boldsymbol{G}$, which consists of the first three columns of matrix $\boldsymbol{A}$, taken with negative sign, and rewrite the Eq. 13 with extended state vector $\boldsymbol{x}^e$ as follows.

$$\boldsymbol{M}\dot{\boldsymbol{x}}^e(t) = \boldsymbol{A}^e\boldsymbol{x}^e(t) + \boldsymbol{B}^e\boldsymbol{u}(t-\tau) + \boldsymbol{G}^e\boldsymbol{V}_{\text{wind}}(t) \tag{48}$$

where the matrices are of the following form

$$\boldsymbol{M} = \left[\begin{array}{c|cccc} \boldsymbol{I}_{13\times13} & \multicolumn{4}{c}{\begin{matrix}\boldsymbol{M}_g \\ \boldsymbol{0}_{7\times4}\end{matrix}} \\ \hline \boldsymbol{0}_{4\times13} & \tau_{u_g} & 0 & 0 & 0 \\ & 0 & \tau_{v_g} & 0 & 0 \\ & k_{q_g}^{u_g} & 0 & \tau_{q_g} & 0 \\ & 0 & k_{r_g}^{v_g} & 0 & \tau_{r_g} \end{array}\right] \tag{49}$$

$$\boldsymbol{A}^e = \left[\begin{array}{c|ccc} \boldsymbol{A} & \boldsymbol{0}_{13\times2} & \boldsymbol{A}_q & \boldsymbol{A}_r \\ \hline \boldsymbol{0}_{4\times13} & \multicolumn{3}{c}{-\boldsymbol{I}_{4\times4}} \end{array}\right] \tag{50}$$

$$\boldsymbol{B}^e = \left[\begin{array}{c} \boldsymbol{B} \\ \hline \boldsymbol{0}_{4\times4} \end{array}\right] \tag{51}$$

$$\boldsymbol{G}^e = \left[\begin{array}{cc} \multicolumn{2}{c}{\boldsymbol{G}} \\ \hline -\boldsymbol{I}_{2\times2} & \boldsymbol{0}_{2\times1} \\ \multicolumn{2}{c}{\boldsymbol{0}_{2\times3}} \end{array}\right] \tag{52}$$

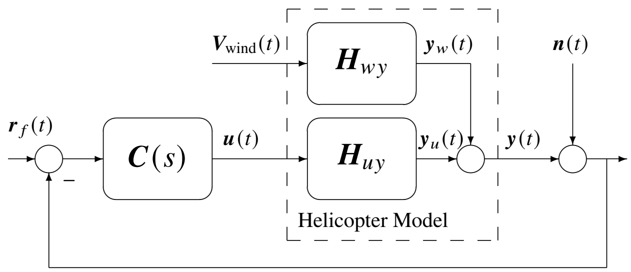

Figure 7. Closed-loop helicopter model

where A_q and A_r are columns of matrix A corresponding to q and r states; $k_{q_g}^{u_g}$, $k_{r_g}^{v_g}$ and M_g are unknown and should be identified. The extended state is

$$x^e = \left[u\; v\; w\; p\; q\; r\; \phi\; \theta\; \psi\; \beta_{1c}\; \beta_{1s}\; \kappa_{1c}\; \kappa_{1s}\; u_g\; v_g\; q_g\; r_g \right]^T \quad (53)$$

Extracting the Spectrum of Response to Gusts

In general, the helicopter model can be represented as shown in Figure 7, where $C(s)$ is a flight controller transfer function, $r_f(t)$ is a reference vector, $n(t)$ is a measurement noise and $y(t)$ is an output vector. The helicopter model has two inputs: the control vector $u(t)$ and the vector of turbulent wind components $V_{\text{wind}}(t)$.

The frequency response function H_{uy} represents the dynamic dependence of the output vector $y(t)$ on the control signals $u(t)$. This is the linear model of the helicopter Eq. 13. A linear model H_{wy} represents the dynamic dependence of the output vector on atmospheric disturbance and is theoretically unknown for hover and low-speed conditions.

Our goal is to find $y_w(\omega)$ in the frequency domain. The noise signal $n(t)$ is not measured in practice. We assume that the signal-to-noise ratio at low-med frequency is high and do not take noise into account. Thus, we can write the equation for $y_w(\omega)$ in the frequency domain as

$$y_w(\omega) = y(\omega) - H_{uy}(\omega)u(\omega) \quad (54)$$

To identify $y_w(\omega)$, we first need to find the complex conjugate. We omit the function argument ω for simplicity of notation.

$$y_w^* y_w^T = y^* y^T - y^* u^T H_{uy}^T - H_{uy}^* u^* y^T + H_{uy}^* u^* u^T H_{uy}^T \quad (55)$$

Taking the expected values of both sides and multiplying by $2/T$ gives the following.

$$\begin{aligned} \hat{G}_{y_w y_w} = \frac{2}{T}\mathbb{E}\left[y_w^* y_w'\right] \quad &= G_{yy} - G_{yu}H_{uy}^T - \\ &-H_{uy}^* G_{uy} + H_{uy}^* G_{uu} H_{uy}^T \end{aligned} \quad (56)$$

where G_{**} are one-sided power spectral density functions and T is the length of the data record. To use Eq. 56 for the linear model of helicopters Eq. 13 in practice, we must define the output vector,

$$y = [\; \dot{u} \quad \dot{v} \quad \dot{w} \quad p \quad q \quad r \quad a_x \quad a_y \quad a_z \quad w\;]^T \quad (57)$$

and the output and direct term matrices.

$$y = Cx + Du \quad (58)$$

Body accelerations in the output vector y can be reconstructed from the measurements (Ref. 21, p. 151). Fill in the matrices in Eq. 56, we should calculate 196 frequency responses. We have chosen the open-loop test for gust spectrum extraction.

The Identification Process

Once $\hat{G}_{y_w y_w}$ is found and $G_{V_{\text{wind}} V_{\text{wind}}}$ is calculated from the wind sensor measurement, we can write the model for identification. This is model Eq. 48 without control input.

$$\begin{aligned} M\dot{x}^e(t) &= A^e x^e(t) + G^e V_{\text{wind}}(t) \\ y_w(t) &= Cx^e(t) + D_w V_{\text{wind}}(t) \end{aligned} \quad (59)$$

where D_w is a direct term matrix composed of the first three rows of the matrix G for linear accelerations and for measurement accelerations.

Since we only have the power spectrum density functions from the flight test and the phase and coherence functions are unknown, we assume that atmospheric disturbances enter the model through the G matrix at low-mid frequencies. For example, a row in the matrix G for the pitch rate q_w contains all three derivatives $[\; M_u \quad M_v \quad M_w\;]$. This means that the amplitude $\hat{G}_{q_w q_w}$ at frequency ω depends on the input of the sum of three components.

$$\begin{aligned} G_{tot}(\omega) = \quad & M_u G_{U_w U_w}(\omega) + M_v G_{V_w V_w}(\omega) + \\ & + M_w G_{W_w W_w}(\omega) \end{aligned} \quad (60)$$

In this way (Ref. 23)

$$\begin{aligned} |H_{U_w q_w}(\omega)|^2 &= \frac{K_u(\omega)\hat{G}_{q_w q_w}(\omega)}{G_{tot}(\omega)} \\ |H_{V_w q_w}(\omega)|^2 &= \frac{K_v(\omega)\hat{G}_{q_w q_w}(\omega)}{G_{tot}(\omega)} \\ |H_{W_w q_w}(\omega)|^2 &= \frac{K_w(\omega)\hat{G}_{q_w q_w}(\omega)}{G_{tot}(\omega)} \end{aligned} \quad (61)$$

where

$$\begin{aligned} K_u(\omega) &= \frac{M_u G_{U_w U_w}(\omega)}{G_{tot}(\omega)} \\ K_v(\omega) &= \frac{M_v G_{V_w V_w}(\omega)}{G_{tot}(\omega)} \\ K_w(\omega) &= \frac{M_w G_{W_w W_w}(\omega)}{G_{tot}(\omega)} \end{aligned} \quad (62)$$

Similarly, we perform the calculations for all components in the matrix G; if there is a zero in the corresponding place, we consider that there is no reaction from this input.

We used the CIFER® software package for identifying the parametric wind model. Since there is no phase information, we fill it with the phase from the model Eq. 47 and amplified the weight on the magnitude cost during identification.

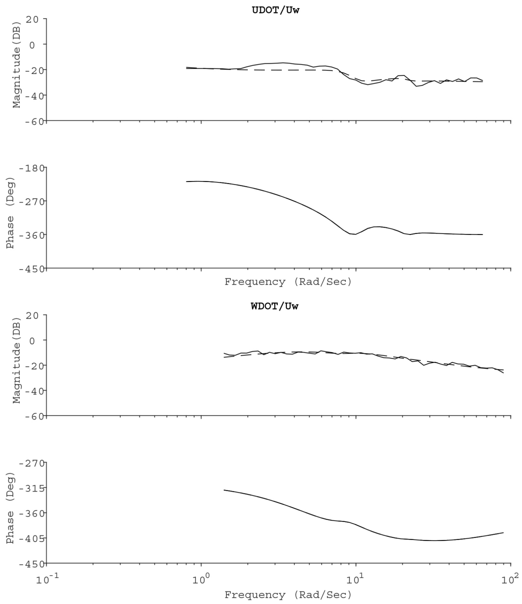

Figure 8. U_w **responses I, solid - test, dashed - identified**

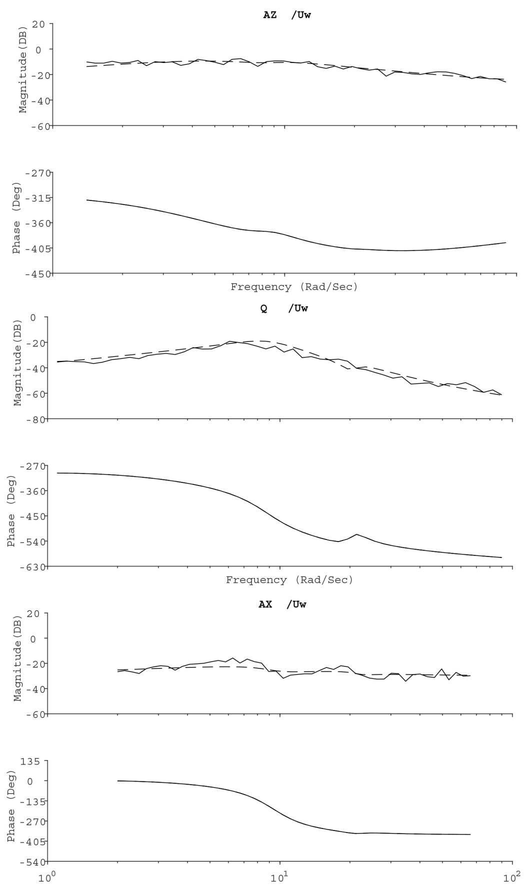

Figure 9. U_w **responses II, solid - test, dashed - identified**

Table 2. Model Identification Cost Function

Frequency response	Cost function
$\dot{u}/U_w$	114.7
$\dot{w}/U_w$	27.5
q/U_w	131.7
a_x/U_w	142.8
a_z/U_w	48.3
$\dot{u}/V_w$	63.4
r/V_w	52.6
a_y/V_w	93.3
The average cost function	77.3

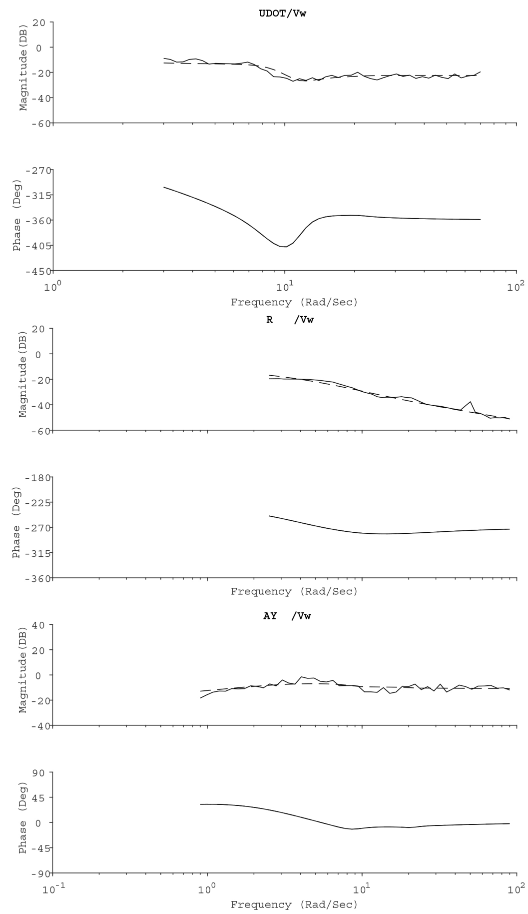

Figure 10. V_w **responses, solid - test, dashed - identified**

Table 3. Identified Wind Model

Parameter	Value
τ_{u_g}	0.189
τ_{v_g}	0.306
τ_{q_g}	0.190
τ_{r_g}	0.175
$k_{q_g}^{u_g}$	0.029
$k_{r_g}^{v_g}$	-0.313

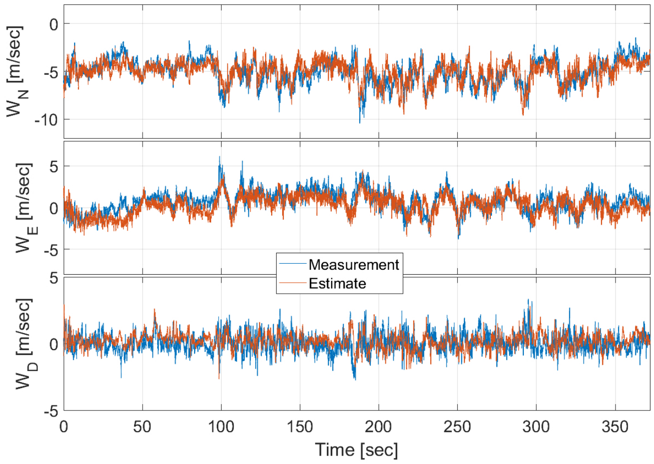

Figure 11. Open-loop test. Estimation with wind model

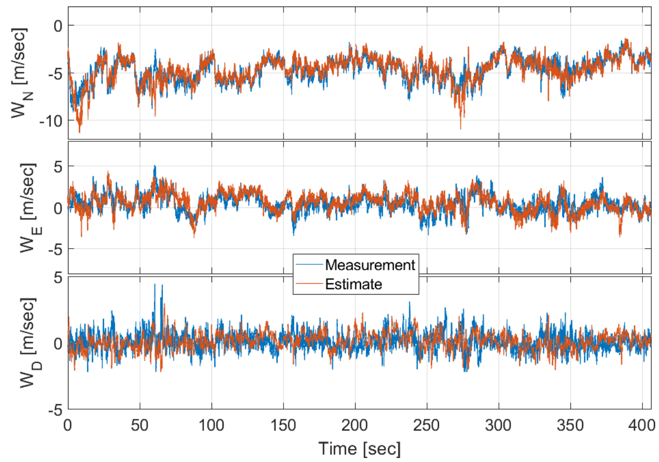

Figure 12. Closed-loop test. Estimation with wind model

Since we have no information on the coherence function, the frequency ranges for identification were chosen where there is good smooth data. The identification results are presented in Table 2 and Figures 8-10. The numerical values of the parameters for the dynamic wind model are given in Table 3, and the interaction matrix for the dynamics of the wind and the aircraft is provided in Eq. 63.

$$\boldsymbol{M}_g = \begin{bmatrix} 0.004 & 0.055 & 0 & -0.007 \\ 0 & 0.122 & 0 & -0.47 \\ 0.067 & 0 & 0.623 & 0 \\ 0 & 0 & 0 & 0 \\ 0.023 & 0 & 0.456 & -0.325 \\ 0 & 0 & 0 & 0 \end{bmatrix} \tag{63}$$

Estimation Method Validation with Dynamic Wind Model

The results of wind estimation with the wind model in the time domain for open and closed loops are shown in Figures 11 and 12, respectively. The improvement is particularly noticeable in the closed-loop test. Peaks of the estimate signal can be observed in Figure 4, which are absent in Figure 12, and the signal here is smoother. Furthermore, the results in the frequency domain are presented in Figures 13 and 14. Using the identified dynamic model, we were able to increase the coincidence frequency of the horizontal wind components to approximately 30 rad/sec. That is enough to determine the characteristics of aviation turbulence, which is defined as the aircraft reaction, i.e., the aircraft's dynamic bandwidth limits it.

Final Results

The final goal of our estimation is to get the wind magnitude and its meteorological direction. For example, the result estimate of $\boldsymbol{W}_0$ obtained using a moving average with a one-minute window for the closed-loop test is shown in Figure 15. On the ground station monitor, the wind is represented by a number inside the circle and the direction is indicated by an arrow on the circle pointing toward the center. In this test, the

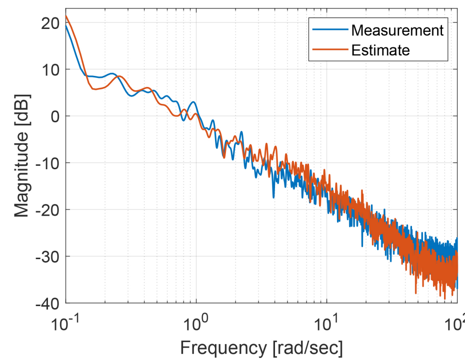

(a) North wind component

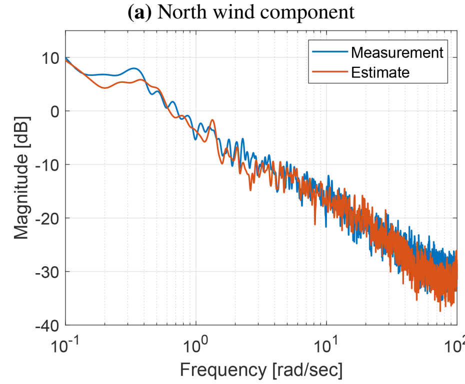

(b) East wind component

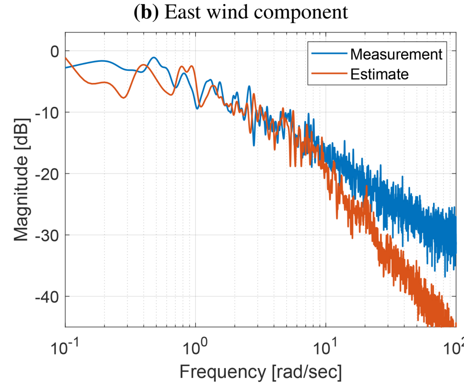

(c) Vertical wind component

Figure 13. Open-loop test. Estimation with wind model

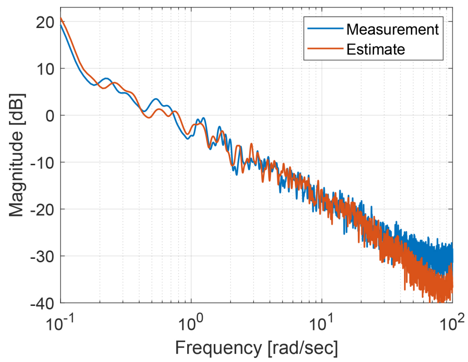

(a) North wind component

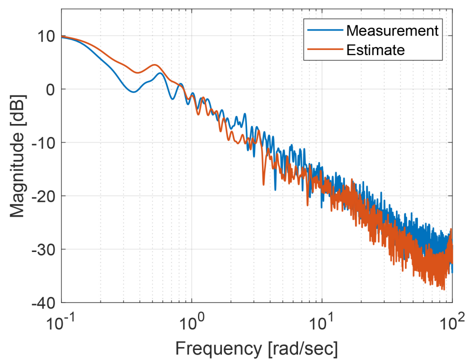

(b) East wind component

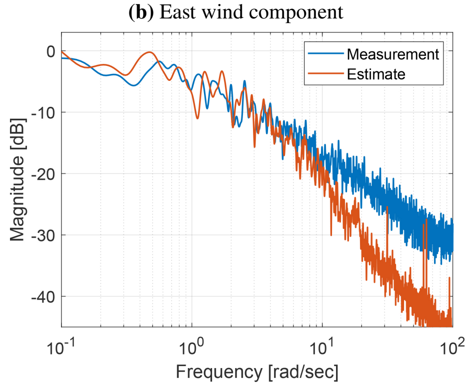

(c) Vertical wind component

Figure 14. Closed-loop test. Estimation with wind model

wind is estimated to be 10 knots with a direction from South by East (SbE) to East. The maximum difference between the wind sensor measurement and the estimate is 0.6 knots and 8.3 degrees in the direction. The root mean square errors are equal to 0.3 knots and 4.2 degrees.

The estimation of aviation turbulence $\boldsymbol{\delta W}(t)$ in the time-domain can be used as a disturbance observer. For turbulence, we can use the moving variance. However, the axes should be chosen first, since the statistical characteristics of turbulence are meaningless in the NED axes. For example, Figure 16 illustrates the statical characteristics of $\boldsymbol{C}_I^B \boldsymbol{\delta W}$ for a one-minute window moving variance for the closed-loop test in the body frame. These estimates can be translated into turbulence intensity levels and shown on the ground station monitor with the appropriate symbol.

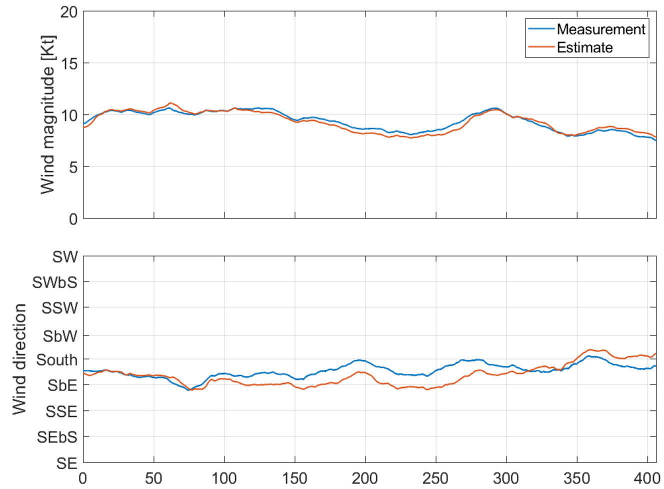

Figure 15. Sustained wind estimate

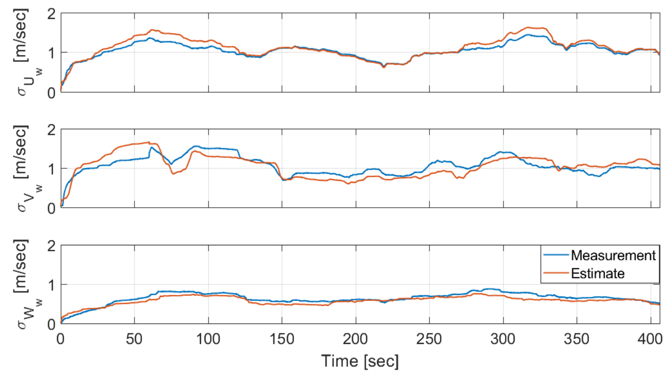

Figure 16. Statistical characteristics of turbulence

Some important practical notes

A helicopter is a vibration-producing machine. First, a vibration test is required, and where peaks are observed, appropriate notch filters should be applied. Otherwise, helicopter vibrations will be evaluated as turbulence effects.

We employed the same concept for calculating aerodynamic forces and moments as used in the model stitching simulation architecture. However, we do not use a look-up table in this paper, but rather only one model that is closest to the current aerodynamic regime. We should also be careful to use the change in the current mass in relation to the base mass for which the linear model was identified, as this is used in model stitching simulation (Ref. 15). Equation Eq. 18 uses the current mass of the helicopter m_c, while the tensor in Eq. 15 includes the base mass value m. The control vector values in the trim also continue to use the basic one $\boldsymbol{U}_0$.

This method is acceptable for small changes in helicopter mass. However, if the mass change is significant, this method of calculating aerodynamic forces and moments can lead to substantial errors and, consequently, errors in wind estimation. Since the torque is nonlinearly dependent on mass, the lateral aerodynamic force from the tail rotor will not be a linear function of the trim position control signal change in Eq. 22. Therefore, we recommend using the trim state vector and control vector for the current mass if the helicopter's current mass differs significantly from its base mass. All the above remarks also apply to changes in air density.

In the estimation algorithm, we explicitly calculate the aerodynamic forces and moments that can be output to the user. Since the aerodynamic moment in steady flight should be zero, this is a good indication of whether the model parameters used $\boldsymbol{X}_0$, $\boldsymbol{U}_0$, $\mathcal{M}$ are acceptable for the wind estimation.

CONCLUSIONS

In this paper, a new practical method for wind estimation is proposed. The following conclusions can be drawn from this work.

1. The study is based on the identified linear helicopter model used for flight control design and utilizes a standard UA sensor kit. Therefore, the practical use of it is straightforward for any UAS project.

2. By employing an Unscented Transform for nonlinear estimation, we can avoid the complexity of computing the Jacobian and utilize the nonlinear model in its original form.

3. The method allows for the estimation of wind speed and direction, as well as the level of turbulence. These data can be downlinked to the ground control station monitor to inform the operator of the critical characteristics of the wind at the current location of the helicopter. Additionally, online estimates in the time domain can serve as a disturbance observer.

4. Since total aerodynamic forces and moments are calculated within the nonlinear process, the accuracy of the mass and air density is crucial for the effectiveness of this method.

5. This method was validated through a hover flight test using measurements from the ultrasonic wind sensor and subsequently improved. The linear dynamical model of the wind effect on the helicopter reaction was identified to improve the estimation of aviation turbulence. Flight tests have shown that sustained wind and its direction can be estimated with an average error in wind strength of 0.3 knots and wind direction of 4.2 degrees using a one-minute moving average window.

6. In the future, the authors plan to validate this model with different wind conditions, specifically when the wind blows from various sides of the helicopter. The authors also plan to continue flight tests and study the relationship between identifying actual atmospheric disturbances and identifying the control equivalent turbulence.

Author contact:

Sergey Nazarov sergey.n@campus.technion.ac.il

Per-Olof Gutman peo@technion.ac.il

REFERENCES

1. Anon. "Unmanned Aircraft System (UAS). Circular 328". Technical report, ICAO, 2011.

2. Mayer S., Hattenberger G., Brisset P., Jonassen M., and Reuder J. "A no-flow-sensor wind estimation algorithm for unmanned aerial systems". *International Journal of Micro Air Vehicles*, 4:15–30, 2012, doi:10.1260/1756-8293.4.1.15.

3. Cho A., Kim J., Lee S., and Kee Ch. "Wind Estimation and Airspeed Calibration using a UAV with a Single-Antenna GPS Receiver and Pitot Tube". *Transactions on Aerospace and Electronic Systems*, 47:109–117, 2011, doi:10.1109/TAES.2011.5705663.

4. Kumar A. and Ben-Tzvi P. "Estimation of Wind Conditions Utilizing RC Helicopter Dynamics". *IEEE/ASME Transactions on Mechatronics*, 24(5):2293–2303, 2019, doi:10.1109/TMECH.2019.2937844.

5. Bergamasco M., Ragazzi A., and Lovera M. "Rotorcraft system identification: a time/frequency domain approach". In *The 19th World Congress, Cape Town, South Africa, August 24-29*, pages 8861–8866. The International Federation of Automatic Control, 2014.

6. Etkin B. *"Dynamics of Atmospheric Flight"*, chapter 13. Wiley, New York, NJ, 1972.

7. Sharman R. and Lane T., editors. *"Aviation Turbulence: Processes, Detection, Prediction"*, chapter 5, pages 97–120. Springer, 2016.

8. Gool P. van. *"Rotorcraft Responses to Atmospheric Turbulence"*. PhD thesis, Delft University, 1997.

9. Mazurov G. I. and Nesteruk V. N. *"The Weather Conditions and Helicopter Flights" (Russian edition)*. Hydrometeoizdat, Saint Petersburg, Russia, 1992.

10. Schafer S. A. "Flight Test Measurement of Ship Airwake Disturbances Using Small-Scale Rotorcraft". Master's thesis, The Pennsylvania State University, 2015.

11. Horn J. F., Bridges D. O., and Lee D. "Flight Control Design for Alleviation of Pilot Workload during Helicopter Shipboard Operations". In *62nd Forum of American Helicopter Society, Phoenix, AZ, May 9-11*, 2006.

12. Cooke M. V. *"Flight Dynamics Principles"*. Elsevier, Waltham, MA, third edition, 2013.

13. Sharman R. and Lane T., editors. *"Aviation Turbulence: Processes, Detection, Prediction"*, chapter 1, pages 3–30. Springer, 2016.

14. Lester Peter F. *"Turbulence: A New Perspecive For Pilots"*. Jeppesen Sanderson Inc., Engiewood, CO, 1993.

15. Tobias E. L. and Tischler M. B. “A Model Stitching Architecture for Continuous Full Flight-Envelope Simulation of Fixed-Wing Aircraft and Rotorcraft from Discrete-Point Linear Models”. Technical report, AMRDEC, Special Report RDMR-AF-16-01, 2016.

16. Nazarov S. and Gutman P.-O. “A Model-based Wind Estimation Method for an Unmanned Helicopter”. In *49th European Rotorcraft Forum, Bückeburg, Germany, September 5-7*, 2023.

17. Gaonkar G. H. and Hohenemser K. H. “An Advanced Stochastic Model for Threshold Crossing Studies of Rotor Blade Vibrations”. *AIAA Journal*, 10(8):1100–1101, 1972, doi:10.2514/3.50309.

18. Julier S. J. and Uhlmann J. K. “Unscented Filtering and Nonlinear Estimation”. *Proceedings of the IEEE*, 92:401 – 422, 04 2004, doi:10.1109/JPROC.2003.823141.

19. Simon D. *“Optimal State Estimation”*. Wiley, Hoboken, NJ, 2006.

20. Julier S. J. “The scaled unscented transformation”. In *Proceedings of the 2002 American Control Conference (IEEE Cat. No.CH37301)*, volume 6, pages 4555–4559, 2002.

21. Tischler M. B. and Remple R. K. *“Aircraft and Rotorcraft System Identification: Engineering Methods with Flight Test Examples”*. AIAA,, Reston, VA, second edition, 2012.

22. Leishman J. G. *“Principles of Helicopter Aerodynamics”*. Cambridge University Press, Cambridge, UK, second edition, 2006.

23. Bendat J. S. and Piersol A. G. *“Random Data”*. Willey, Hoboken, NJ, fourth edition, 2010.